Temperature and density dependence of asymmetric nuclear matter and protoneutron star properties within an extended relativistic mean field model

Gulshan Mahajan[1,2,*] and Shashi K. Dhiman[1,3,†]

[1]*Department of Physics, Himachal Pradesh University, Shimla 171005, India*

[2]*Department of Physics, R.G.M. Government College, Joginder Nagar 175015, India*

[3]*University Institute of Natural Sciences and Interface Technologies, Himachal Pradesh Technical University, Post Box 12, Hamirpur, Pin 177001, India*

(Received 14 June 2011; published 11 October 2011)

The effect of temperature and density dependence of the asymmetric nuclear matter properties is studied within the extended relativistic mean field (ERMF) model, which includes the contribution from the self and mixed interaction terms by using different parametrizations obtained by varying the neutron skin thickness Δr and ω-meson self-coupling (ζ). We observed that the symmetry energy and its slope and incompressibility coefficients decrease with increasing temperatures up to saturation densities. The ERMF parametrizations were employed to obtain a new set of equations of state (EOS) of the protoneutron star (PNS) with and without inclusion of hyperons. In our calculations, in comparison with cold compact stars, we obtained that the gravitational mass of the protoneutron star with and without hyperons increased by $\sim 0.4 M_{\odot}$ and its radius increased by ~ 3 km. Whereas in case of the rotating PNS, the mass shedding limit decreased with increasing temperature, and this suggested that the keplerian frequency of the PNS at $T = 10$ MeV should be smaller by 14%–20% for the EOS with hyperon, as compared to the keplerian frequency of a cold compact star.

DOI: 10.1103/PhysRevC.84.045804 PACS number(s): 26.60.−c, 21.65.Cd, 97.10.Kc, 97.10.Nf

I. INTRODUCTION

The behavior of nuclear matter at high density and finite temperature is one of the challenging problems in contemporary modern nuclear physics. Among the successful and widely used approaches to study nuclear matter are nonrelativistic mean field theory, with effective nucleon-nucleon interactions such as skyrme forces [1–3], and relativistic mean field (RMF) theory [4]. The RMF theory is more fundamental as it starts from hadronic field theory with strongly interacting baryons and mesons as degrees of freedom [5], and it describes very well the basic properties of nuclei near the valley of stability [6] and the properties of exotic nuclei with large numbers of neutrons or protons [7]. The properties of cold nuclear matter can be studied by imposing the constraints of bulk nuclear matter properties at the saturation density $\rho_0 = 0.16$ fm^{-3}; recent experimental limits establish the following values: symmetry energy $E_{\rm sym} = 30 \pm 5$ MeV [8,9], slope of symmetry energy $L = 88 \pm 25$ MeV [10], and incompressibility coefficient $K = 240 \pm 20$ MeV [11–13]. It is considered theoretically that the density dependence of symmetry energy can be represented by $E_{\rm sym}(\rho_0) = 31.6(\rho/\rho_0)^{\gamma}$, with $\gamma = 0.69$–1.05 at subnormal density [10], which led to the extraction of a value for the slope of the nuclear symmetry energy of $L = 88 \pm 25$ MeV. This symmetry energy value is also in harmony with the symmetry energy obtained from the isoscaling analysis of the isotope ratio in intermediate energy heavy-ion collisions [14].

Recently, heavy-ion reactions induced in laboratories have provided the atmosphere necessary to produce hot neutron-rich matter similar to that existing in astrophysical situations. The reactions especially, which are induced by radioactive beams, provide a unique means to investigate the isospin-dependent properties of asymmetric nuclear matter at the Cooling Storage Ring (CSR) at HIRFL in China, the Radioactive Ion Beam (RIB) at RIKEN in Japan, FAIR/GSI in Germany, SPIRAL2/GANIL in France, the Facility for Rare Isotope Beam (FRIB) in the United States. The heavy-ion collision data from analyzing isospin diffusion and size of the neutron skin in ^{208}Pb [4,10] have helped us significantly in understanding symmetry energy. The symmetry energy of hot neutron-rich matter in a low-density regime [15] is important for understanding the liquid-gas phase transition of asymmetric nuclear matter, the dynamical evolution of massive stars, and the supernova explosion mechanism. The density dependence of symmetry energy influences the nature and stability of the phases of compact star (CS), the feasibility of direct URCA cooling process within interior of CS, the composition and thickness of inner crust of CS, the frequency of its crustal vibrations and radius of CS. Many correlations have been studied to understand the density behavior of symmetry energy [16]. However, the fundamental origin of this apparent evolution of symmetry energy is still not clear, and it is particularly important to understand to what degree its evolution depends on the density and /or temperature of nuclear matter. Apart from symmetry energy, the nuclear matter equations of state (EOS) also depend upon the values of incompressibility [17]. In recent times the giant monopole resonance has made it possible to find the value of incompressibility [18]. Accurate knowledge of the density and temperature dependence of symmetry energy and incompressibility can lead to plausible EOS of the asymmetric matter.

The properties of the compact stars are mainly determined by the EOS of nuclear dense matter, which is charge neutral matter in β equilibrium [19]. Any given EOS of baryonic matter determines uniquely the mass-radius relationship of a

*gul.mahajan@yahoo.co.in

†shashi.dhiman@gmail.com

compact star and, in particular, the maximum mass a compact star can achieve before collapsing into a black hole [20]. Theoretical investigations of high-density β-stable have lead to the conclusion that hyperons will appear at densities of about 2–4 times the saturation density (ρ_0) and soften the EOS in high-density regimes, as the conversion of nucleons to hyperons can relieve the fermi surface and leads to a reduction of compact star mass [21,22]. For compact star matter with uniform distribution, the composition is determined by the requirement of charge neutrality and β-equilibrium conditions. The threshold density for a hyperon species is determined not only by its charge and mass but also by the meson fields. The stiffer the EOS without hyperons is, the greater is the softening effect when hyperons are included [20,23]. Further the presence of hyperons should allow direct URCA-like cooling involving the β decay of the hyperons.

In this work we have extended our previous ERMF model [24] to study the effect of temperature on asymmetric nuclear matter and the properties of protoneutron stars (PNS). This paper is organized as follows. In Sec. II we briefly describe the extended relativistic mean field theory. In Sec. III we present the result and discussion for nuclear matter properties, structure properties of non rotating PNS and, rotating PNS with keplerian frequency. In Sec. IV we present our conclusions for the present work.

II. FORMALISM

The Lagrangian density for the ERMF model describes the interactions from self and mixed terms for the scalar-isoscalar (σ), vector-isoscalar (ω), and vector-isovector (ρ) mesons [24,25]. For completeness the Lagrangian density for the extended ERMF model can be written as

$$\mathcal{L} = \mathcal{L}_{\mathcal{BM}} + \mathcal{L}_{\sigma} + \mathcal{L}_{\omega} + \mathcal{L}_{\rho} + \mathcal{L}_{\sigma\omega\rho}. \tag{1}$$

The description of the various terms of the Lagrangian and the Euler-Lagrangian equations for ground-state expectation values of the meson fields are provided in Ref. [24]. At finite temperatures the baryon vector density ρ_B, scalar density ρ_{sB} and charge density ρ_p are, respectively,

$$\rho_B = \langle \overline{\Psi}_B \gamma^0 \Psi_B \rangle (n_i - \overline{n_i}) = \frac{\gamma}{(2\pi)^3} \int_0^{k_B} d^3k (n_i - \overline{n_i}), \tag{2}$$

$$\begin{aligned} \rho_{sB} &= \langle \overline{\Psi}_B \Psi_B \rangle (n_i + \overline{n_i}) \\ &= \frac{\gamma}{(2\pi)^3} \int_0^{k_B} d^3k \frac{M_B^*}{\sqrt{k^2 + M_B^{*2}}} (n_i + \overline{n_i}), \end{aligned} \tag{3}$$

$$\rho_p = \left\langle \overline{\Psi}_B \gamma^0 \frac{1 + \tau_{3B}}{2} \Psi_B \right\rangle (n_i + \overline{n_i}). \tag{4}$$

Here, γ is the spin-isospin degeneracy. $M_B^* = M_B - g_{\sigma B}\sigma - g_{\sigma^* B}\sigma^*$ is the effective mass of the baryon species $B = (p, n, \Lambda, \Sigma^{\pm}, \Xi^{\pm})$, k_B is its Fermi momentum, and τ_{3B} denotes the isospin projections of baryon B.

The thermal distribution functions in these expressions are defined by

$$n_i = \frac{1}{e^{\beta(\epsilon_i^* - \nu_i)} + 1} \quad \text{and} \quad \overline{n_i} = \frac{1}{e^{\beta(\epsilon_i^* + \nu_i)} + 1}, \tag{5}$$

where

$$\begin{aligned} \epsilon_i^* &= \sqrt{k^2 + M_B^{*2}} \\ \text{and} \quad \nu_i &= \mu_i - g_{\omega N}\omega \pm g_{\rho}\frac{\rho}{2} \qquad (i = n, p) \end{aligned} \tag{6}$$

are the effective energy and effective chemical potential, respectively.

The energy density of the uniform matter in the ERMF models is given by

$$\begin{aligned} \mathcal{E} = {} & \sum_{j=p,n} \frac{1}{\pi^2} \int_0^{k_j} \epsilon_i^*(k) k^2 dk (n_i + \overline{n_i}) + \sum_B g_{\omega B}\omega\rho_B + \sum_B g_{\rho B}\tau_{3B}\rho + \frac{1}{2}m_\sigma^2\sigma^2 \\ & + \frac{\overline{\kappa}}{6}g_{\sigma N}^3\sigma^3 + \frac{\overline{\lambda}}{24}g_{\sigma N}^4\sigma^4 - \frac{\zeta}{24}g_{\omega N}^4\omega^4 - \frac{\xi}{24}g_{\rho N}^4\rho^4 - \frac{1}{2}m_\omega^2\omega^2 - \frac{1}{2}m_\rho^2\rho^2 \\ & - \overline{\alpha_1}g_{\sigma N}g_{\omega N}^2\sigma\omega^2 - \frac{1}{2}\overline{\alpha_1}' g_{\sigma N}^2 g_{\omega N}^2 \sigma^2\omega^2 - \overline{\alpha_2}g_{\sigma N}g_{\rho N}^2\sigma\rho^2 - \frac{1}{2}\overline{\alpha_2}' g_{\sigma N}^2 g_{\rho N}^2 \sigma^2\rho^2 \\ & - \frac{1}{2}\overline{\alpha_3}' g_{\omega N}^2 g_{\rho N}^2 \omega^2\rho^2 + \frac{1}{2}m_{\sigma^*}^2\sigma^{*2} + \sum_B g_{\phi B}\phi\rho_B - \frac{1}{2}m_\phi^2\phi^2. \end{aligned} \tag{7}$$

The pressure of the uniform matter is given by

$$\begin{aligned} P = {} & \sum_{j=p,n} \frac{1}{3\pi^2} \int_0^{k_j} \frac{k^4 dk}{\sqrt{k^2 + M_j^{*2}}} (n_i + \overline{n_i}) - \frac{1}{2}m_\sigma^2\sigma^2 - \frac{\overline{\kappa}}{6}g_{\sigma N}^3\sigma^3 - \frac{\overline{\lambda}}{24}g_{\sigma N}^4\sigma^4 \\ & + \frac{\zeta}{24}g_{\omega N}^4\omega^4 + \frac{\xi}{24}g_{\rho N}^4\rho^4 + \frac{1}{2}m_\omega^2\omega^2 + \frac{1}{2}m_\rho^2\rho^2 + \overline{\alpha_1}g_{\sigma N}g_{\omega N}^2\sigma\omega^2 \\ & + \frac{1}{2}\overline{\alpha_1}' g_{\sigma N}^2 g_{\omega N}^2 \sigma^2\omega^2 + \overline{\alpha_2}g_{\sigma N}g_{\rho N}^2\sigma\rho^2 + \frac{1}{2}\overline{\alpha_2}' g_{\sigma N}^2 g_{\rho N}^2 \sigma^2\rho^2 \\ & + \frac{1}{2}\overline{\alpha_3}' g_{\omega N}^2 g_{\rho N}^2 \omega^2\rho^2 - \frac{1}{2}m_{\sigma^*}^2\sigma^{*2} + \frac{1}{2}m_\phi^2\phi^2. \end{aligned} \tag{8}$$

The symmetry energy $E_{\rm sym}$, the slope L, and the incompressibility K can be evaluated as

$$E_{\rm sym}(\rho) = \frac{1}{2}\frac{d^2E(\rho,\delta)}{d\delta^2}\bigg|_{\delta=0}, \tag{9}$$

$$L = 3\rho_0\frac{dE_{\rm sym}(\rho)}{d\rho}\bigg|_{\delta=\rho_0}, \tag{10}$$

$$K = 9\rho_0^2\frac{d^2E_0(\rho)}{d\rho^2}\bigg|_{\rho=\rho_0}, \tag{11}$$

where ρ_0 is the saturation density, $E(\rho,\delta)$ is the energy per nucleons at a given density ρ and asymmetry parameter $\delta = (\frac{\rho_n-\rho_p}{\rho_n+\rho_p})$, and $E_0(\rho) = E(\rho,\delta=0)$ is the energy per nucleon for symmetric matter.

III. RESULTS AND DISCUSSION

In the present work we have employed parametrization sets of the ERMF model, BSR1–BSR21 [24,26], generated by varying the ω-meson self-coupling ζ and neutron skin thickness Δr for the ^{208}Pb nucleus. These parametrizations have been obtained so as to reproduce the nuclear structure properties in finite nuclei and the bulk properties of nuclear matter at nuclear saturation density [24]. The parametrization sets BSR1–BSR7 correspond to the value of ω-meson self-coupling $\zeta = 0.0$, sets BSR8–BSR14 correspond to $\zeta = 0.03$, and sets BSR15–BSR21 correspond to $\zeta = 0.06$, and for each parametrization set the value of neutron skin thickness of ^{208}Pb varies from 0.16 to 0.28 fm in intervals of 0.02 fm. Further, the hyperon-meson coupling parameters are expressed in terms of the nucleon-meson coupling using the SU(6) model. The coupling parameters of σ-meson–hyperon and ω-meson–hyperon are very sensitive to structural properties of compact stars, so these parameters have been fitted to the hyperon-nucleon potential depth the same as in Ref. [24], and its value $X_{\omega y}$ varies from 0.5 to 0.8, where $X_{\omega y}$ is defined as

$$X_{\omega Y} = \begin{cases} \left(\frac{g_{\omega Y}}{g_{\omega N}}\right) & \text{for } \Lambda \text{ and } \Sigma \text{ hyperons,} \\ 2\left(\frac{g_{\omega Y}}{g_{\omega N}}\right) & \text{for } \Xi \text{ hyperons,} \end{cases} \tag{12}$$

where $g_{\omega Y}$ and $g_{\omega N}$ are the ω-meson–hyperon and ω-meson–nucleon coupling parameters.

A. Nuclear matter properties

We study the properties of symmetric and asymmetric nuclear matter for different parametrizations of the ERMF model at temperatures of 0 to 30 MeV. In Table I we present the results for the bulk properties of nuclear matter at saturation density for the parameters BSR1, BSR7, BSR8,

TABLE I. The bulk properties of the nuclear matter at the saturation density (ρ_0) for the different temperatures, saturation density (ρ_0), energy per nucleon (E/A), incompressibility coefficient for symmetric nuclear matter (K), symmetry energy [$E_{\rm sym}(\rho_0)$], linear density dependence of symmetry energy (L), and effective nucleon mass/nucleon mass (M_N^*/M_N).

Force	ζ	Δr (fm)	T MeV	ρ_0 (fm^{-3})	E/A (MeV)	K (MeV)	$E_{\rm sym}(\rho_0)$ (MeV)	L (MeV)	M_N^*/M_N
BSR1	0.00	0.16	0	0.1481	−16.0192	240.0477	30.9841	59.6144	0.6052
			10	0.1481	−16.0192	240.0477	30.9841	59.6144	0.6052
			20	0.1481	−16.0194	239.7282	30.9838	59.6240	0.6052
			30	0.1464	−16.0483	211.0066	30.7468	59.3789	0.6088
BSR7	0.00	0.28	0	0.1493	−16.1753	231.8574	36.9894	98.7838	0.6014
			10	0.1493	−16.1753	231.8574	36.9894	98.7838	0.6014
			20	0.1493	−16.1755	231.5692	36.9890	98.7972	0.6014
			30	0.1478	−16.2010	204.8214	36.6289	98.4333	0.6048
BSR8	0.03	0.16	0	0.1469	−16.0351	230.8656	31.0094	60.3747	0.6059
			10	0.1469	−16.0351	230.8656	31.0094	60.3747	0.6059
			20	0.1469	−16.0353	230.5972	31.0092	60.3831	0.6059
			30	0.1455	−16.0643	207.6021	30.8013	60.2005	0.6087
BSR14	0.03	0.28	0	0.1474	−16.1838	235.4955	36.0527	93.4748	0.6078
			10	0.1474	−16.1838	235.4955	36.0527	93.4748	0.6078
			20	0.1474	−16.1840	235.2218	36.0523	93.4878	0.6078
			30	0.1459	−16.2150	212.2077	35.7080	93.2011	0.6106
BSR15	0.06	0.16	0	0.1456	−16.0320	226.9275	30.9177	61.8943	0.6075
			10	0.1456	−16.0320	226.9275	30.9177	61.8943	0.6075
			20	0.1455	−16.0322	226.4806	30.9002	61.8556	0.6077
			30	0.1442	−16.0621	209.2170	30.7094	61.7048	0.6098
BSR21	0.06	0.28	0	0.1452	−16.1235	220.4414	35.7123	92.5457	0.6017
			10	0.1452	−16.1235	220.4414	35.7123	92.5457	0.6017
			20	0.1451	−16.1236	220.0422	35.6861	92.4886	0.6019
			30	0.1441	−16.1486	205.8949	35.4542	92.3135	0.6036

BSR14, BSR15, and BSR21 at temperatures $T = 0$, 10, 20, and 30 MeV. It is found that the bulk properties at saturation densities remain almost the same up to 20 MeV, but as temperature increases further these properties start varying significantly. The results for the saturation density (ρ_0), energy per nucleon (E/A), incompressibility coefficient for symmetric nuclear matter (K), symmetry energy [$E_{\rm sym}(\rho_0)$], linear density dependence of symmetry energy slope (L), and effective nucleon mass (M^*) for the various parametrizations at saturation density are given in Table I. It can be seen from Table I that the nuclear matter properties at saturation density such as energy per nucleon, symmetry energy and value of its slope, and the effective mass of the nucleons get changed beyond $T \geqslant 20$ MeV by a very small amount with respect to $T = 0$ MeV for the all parametrizations of the ERMF model. However, the incompressibility coefficient for symmetric nuclear matter decreases up to a maximum of 12.5% at $T = 30$ MeV with respect to $T = 0$ MeV for the BSR1 parametrization, which provides the stiffest EOS with neutron star gravitational mass $M = 2.5M_\odot$ [24]. The variation in the values of K is a minimum of 7% for the BSR21 parametrization, which provides the softest EOS with neutron star gravitational mass $M = 1.74M_\odot$ [24].

The nuclear symmetry energy is a fundamental input to understand the exotic nuclei, heavy-ion collision data, and many other astrophysical phenomena. Therefore, recently many efforts have been made to extract the information on the magnitude and density dependence of symmetry energy of nuclear matter. In Fig. 1 we present the values of $E_{\rm sym}(\rho_0)$

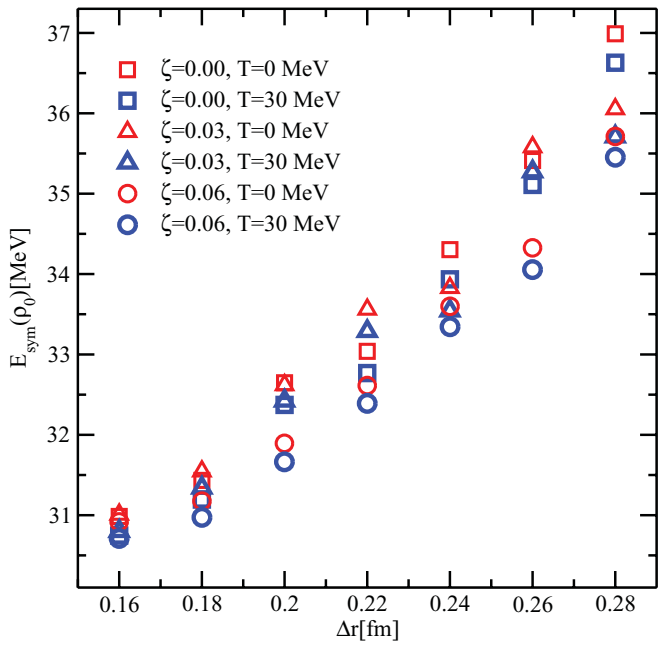

FIG. 1. (Color online) The symmetry energy $E_{\rm sym}(\rho_0)$ plotted as a function of the neutron skin thickness Δr in the ^{208}Pb nucleus for 21 different parametrizations of the ERMF model. The squares, triangles, and circles represent results for the parametrizations BSR1–BSR7, BSR8–BSR14, and BSR15–BSR21, respectively. The red symbols represent the results at $T = 0$ MeV and the blue symbols represent the results at $T = 30$ MeV.

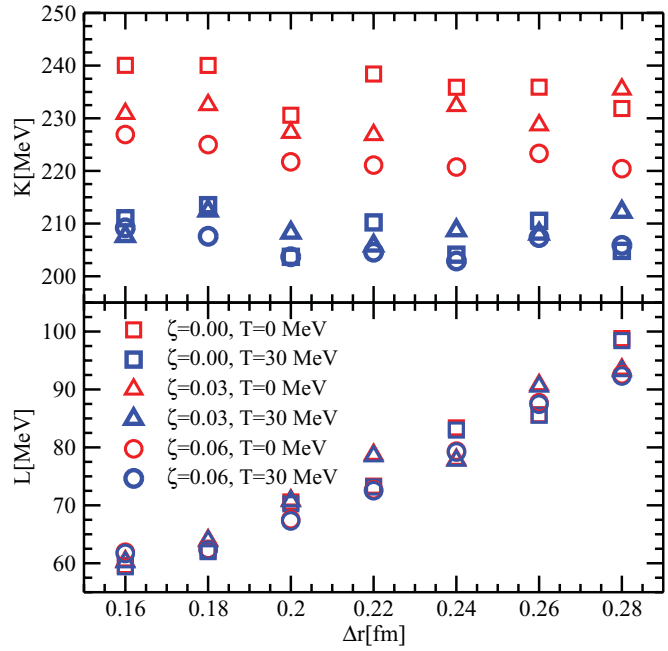

FIG. 2. (Color online) Same as Fig. 1, but for the slope of the symmetry energy (L) and incompressibility coefficient (K) of nuclear matter.

at saturation density as a function of Δr, the neutron skin thickness in the ^{208}Pb nucleus for various model parametrizations, the squares represent the parametrizations BSR1–BSR7 with $\zeta = 0.00$, the triangles represent the parametrizations BSR8–BSR14 with $\zeta = 0.03$, and the circles represent the parametrizations BSR15–BSR21 with $\zeta = 0.06$. In Fig. 2, in the lower panel we present the slope of symmetry energy and in the upper panel we present the incompressibility coefficient for nuclear matter as a function of Δr. In Figs. 1 and 2 the red symbols represent the results at $T = 0$ MeV and the blue symbols represent the results at $T = 30$ MeV. It is found that variation in the values of symmetry energy becomes reasonably large as the value of neutron skin thickness increases, whereas the value for the slope of symmetry energy remains unaffected at $T = 0$ and 30 MeV. The value of incompressibility coefficient is sensitive to ζ and indicates the change at $T = 30$ MeV.

In Fig. 3 we compare the density dependence of the incompressibility coefficient at finite temperatures for various parametrizations with cold nuclear matter. It is found that the incompressibility coefficient at finite temperature has shown change below neutron saturation densities of $\rho_0 = 0.15$ fm^{-3} only and K gain maximum value in the range of densities $\sim$0.4 to 0.5 fm^{-3}. The maximum value is very sensitive to ζ, remains almost same on varying Δr, and decreases with increasing temperature. Further, we explore the effect of density on energy per nucleon (E/A) for symmetric nuclear matter and pure neutron matter at finite temperatures as shown in Fig. 4, computed by employing the BSR1, BSR7, BSR15, and BSR21 parametrizations. At the finite temperature the E/A for symmetric nuclear matter decreases sharply as compared to the E/A for pure neutron matter in the low-density regime, and with the increase of ζ from 0.00 to 0.06, the E/A

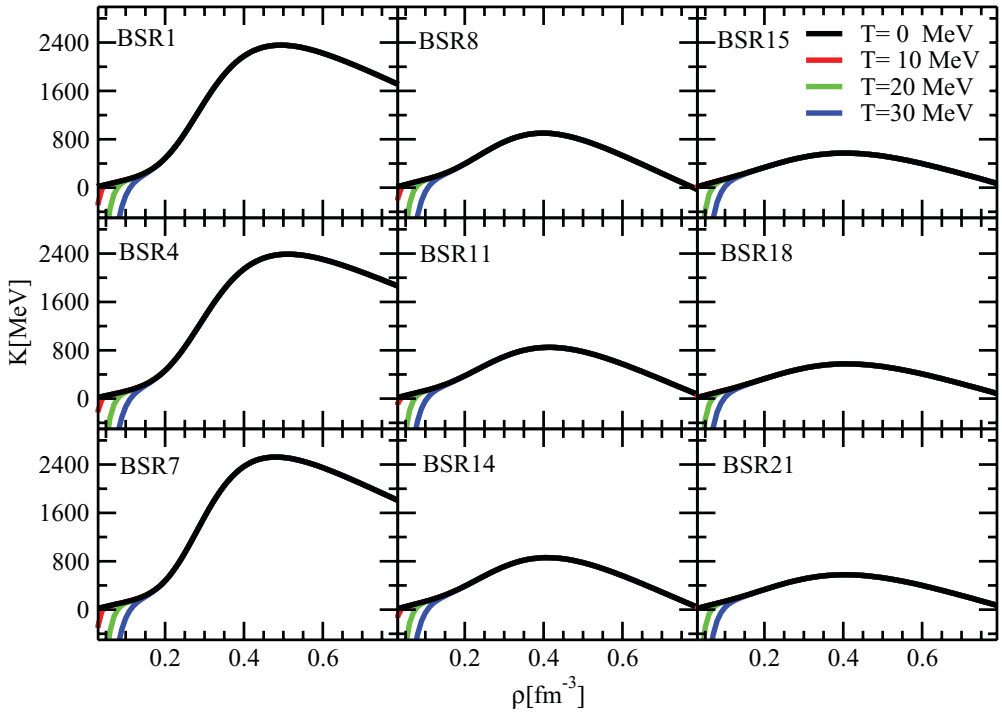

FIG. 3. (Color online) The density dependence of the incompressibility coefficient is plotted at temperatures of 0, 10, 20, and 30 MeV for various parametrizations.

of both symmetric nuclear matter and pure neutron matter decreases moderately. The E/A remains almost unchanged for the variation in values of Δr in ^{208}Pb. In Fig. 5 we present the variation of E/A as a function of density at the different values of the asymmetry parameter δ at $T = 0$, 5, 10, and 20 MeV for the BSR15 parametrization. The value of E/A increases reasonably well with the increase in value of δ. Figure 5 shows that the E/A changes in the higher-density region due to the change in the asymmetry parameter δ,

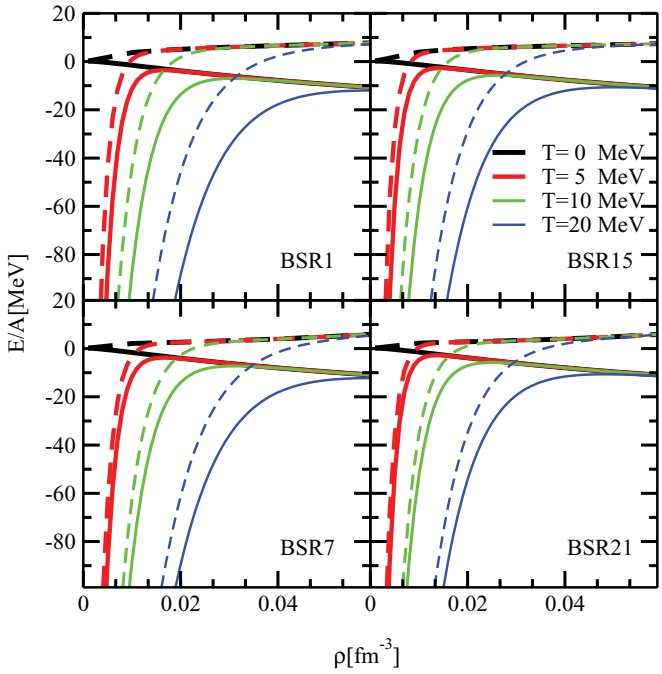

FIG. 4. (Color online) The variation in energy per nucleon (E/A) for symmetric nuclear matter (solid lines) and for pure neutron matter (dashed lines) calculated with the BSR1, BSR7, BSR15, and BSR21 parametrizations is plotted as a function of density at temperatures of 0, 5, 10, and 20 MeV.

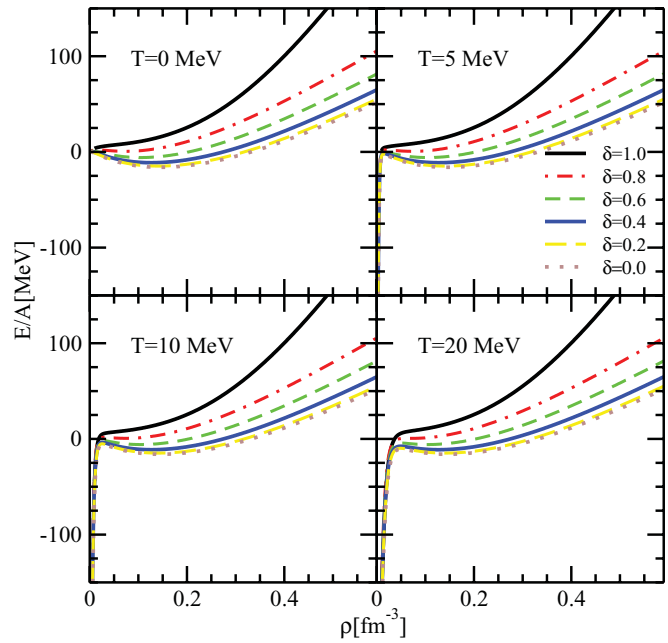

FIG. 5. (Color online) The variation in energy per nucleon (E/A) for asymmetric nuclear matter at temperatures of 0, 5, 10, and 20 MeV with various values of δ calculated with the BSR15 parametrization.

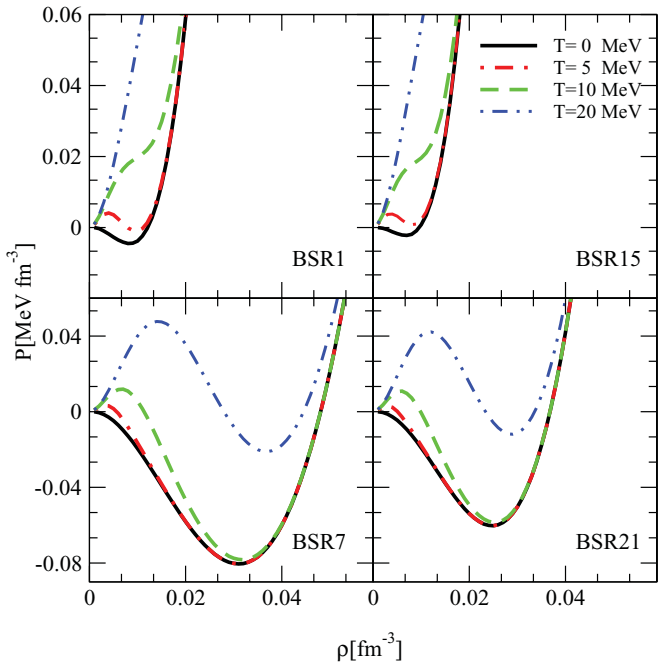

FIG. 6. (Color online) The pressure for symmetric nuclear matter for the BSR1, BSR7, BSR15, and BSR21 parametrizations is plotted as a function of density at temperatures of 0, 5, 10, and 20 MeV.

whereas in the low-density region E/A varies with increases in temperature.

In Fig. 6 we present the variation of the EOS of symmetric nuclear matter as a function of nuclear matter density at various temperatures for the BSR1, BSR7, BSR15, and BSR21 parametrizations, in the very-low-density region. The pressure varies with temperatures at small values of densities and has negligible effect at higher densities. The variation in pressure for a given density depends mostly on the choice of parametrizations and temperature. The pressure become negative for BSR7 and BSR21 parametrizations with $\Delta r =$ 0.28 fm, in the low density regime ($\rho \leqslant 0.04$ fm^{-3}). In Fig. 7 the pressure of asymmetric nuclear matter is plotted as a function of density in the low-density region for various values of the asymmetry parameter δ. The solid line represents $T =$ 0 MeV and the dashed line represents $T = 20$ MeV. The black line, red line, green line, and blue line represent the BSR1, BSR7, BSR15, and BSR21 parametrizations, respectively. The EOS becomes stiff with the increase in the asymmetry parameter δ and trend continues till it becomes pure neutron matter.

We study the density dependence of symmetry energy, nuclear matter pressure density, and energy per nucleon at low density and the nuclear matter incompressibility coefficient as a function of density with different RMF models. The comparison of the theoretical results for $E_{\rm sym}$, P, E/A, and K computed with BSR11 with NL3 [27] and TM1 [28] parametrizations of RMF theory at temperatures of 0 and 30 MeV as a function of density are presented in Fig. 8. The solid and dashed black lines represent the results of the BSR11 parametrization, the red lines represent the NL3 parametrization, and the blue lines represent the TM1 parametrization. The solid lines and dashed lines represent temperatures of 0 and 30 MeV, respectively. It is found that the values of $E_{\rm sym}$, P, E/A, and K are very sensitive to temperature at lower densities (∼0–0.1 fm^{-3}) and are independent of temperature at higher densities. Further, we find a reasonable change in the behavior of the symmetry energy for small values of Δr. However, the symmetry energy decreases at 30 MeV, and at very low density (∼0.02 fm^{-3}) for the value of $E_{\rm sym}$ the trend reverses as shown in Fig. 8. It is noteworthy from Fig. 8 that, except for nuclear matter incompressibility computed with the NL3 parametrization, all other RMF parametrizations yield almost the same values of bulk properties.

B. Nonrotating PNS

We discuss the properties of PNS composed of charge neutral nuclear matter at different temperatures. The fixed total baryon density is given as

$$\rho = \sum_B \rho_B, \tag{13}$$

the charge neutrality condition is given as

$$\sum_B q_B \rho_B + \sum_L q_L \rho_L = 0, \tag{14}$$

and the chemical equilibrium conditions,

$$\mu_B = \mu_N - q_B \mu_e, \tag{15}$$

$$\mu_\mu = \mu_e, \tag{16}$$

are satisfied. For density higher than $0.5\rho_0$ the baryonic part of the EOS is evaluated within the ERMF model, whereas the contributions of the electrons and muons to the EOS are evaluated within the Fermi gas approximation. At densities lower than $0.5\rho_0$ down to $0.4 \times 10^{-10}\rho_0$ we use the EOS of Baym *et al.* [29]. The properties of nonrotating compact star are obtained by integrating the Tolman-Oppenheimer-Volkoff equations [30].

Figure 9 shows the relative particle fraction calculated at different temperatures for the BSR15 parametrization as a function of density. At finite temperature, neutrons, protons, Λ hyperons, and electrons become abundant at baryon density lower than their particle threshold density in the cold nuclear matter, whereas Ξ hyperons disappear even at $T = 3$ MeV and the particle threshold densities of muons and Σ hyperons increase to 0.902 and 0.5 fm^{-3}, respectively, as compared with their threshold densities in cold nuclear matter. In our calculation, the threshold densities of hyperons in cold matter are as follows: for Λ hyperons the threshold density is 0.376 fm^{-3}, for Σ^- hyperons it is 0.482 fm^{-3}, and for Ξ^-hyperons it is 0.490 fm^{-3}, but at $T = 10$ MeV the threshold density of Λ hyperons decreases to 0.112 fm^{-3}, of Σ^- hyperons it increases to 0.902 fm^{-3}, and for Ξ^- it disappears as shown in Fig. 9. We also observed the effect of temperature on relative particle fraction in compact stars without hyperons. It is found that with the increase in temperature the neutrons, protons, and leptons become abundant at lower densities; however, at higher densities for

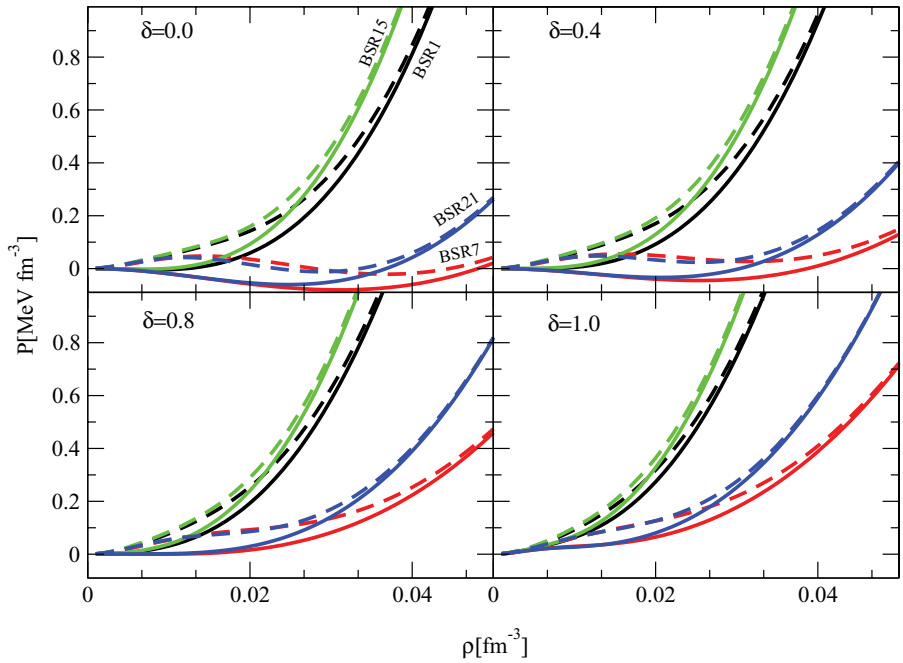

FIG. 7. (Color online) The pressure of asymmetric nuclear matter plotted as a function of density in low-density regions for various values of the asymmetry parameter δ. The solid line represents $T = 0$ MeV and the dashed line represents $T = 20$ MeV. The black line, red line, green line, and blue line represent the BSR1, BSR7, BSR15, and BSR21 parametrizations, respectively.

protons, electrons, and muons, the magnitude of the particle fraction slightly decreases. The pressure density is plotted as a function of baryon density by employing BSR1, BSR8, and BSR15 parametrizations as shown in Fig. 10. The dashed lines represent EOS with hyperons having hyperon-meson coupling parameter $X_{\omega y} = 0.50$ and the solid lines represent EOS without hyperons at temperatures of $T = 0$, 3, 5, and 10 MeV. The EOS become stiff at higher temperature with and without inclusion of hyperons and, subsequently, there is an increase in the gravitational mass of the CS.

In Fig. 11 we present the gravitational mass and radius relationship for the PNS. The dashed lines represent mass for EOS with hyperons at $X_{\omega y} = 0.50$ and the solid lines represent mass for EOS without hyperons at temperatures of 0, 3, 5, and 10 MeV. The region excluded by causality (green solid line) and rotation constraints of compact star XTE J1739-285 (maroon solid line) are shown in the upper left panel. The mass and radius limit estimate from Vela pulsar glitches $\Delta I/I = 0.014$ is shown as the magenta solid line in the upper left panel. The recent mass measurement of the PSR J1614-2230 pulsar of 1.97 ± 0.04 [31] is displayed in Fig. 11 as another constraint to the nuclear matter EOS, computed by our group in Ref. [24]. The EOS that contain exotic hadronic matter of hyperons does not satisfy the mass constrain of the PSR J1614-2230 as shown in Fig. 11, and also as discussed similar in Ref. [31] that the model of EOS includes the appearance of hyperons or kaon condensates. However the EOS computed [24] without hyperons for $\zeta = 0.00$ and $\zeta = 0.03$ satisfy the

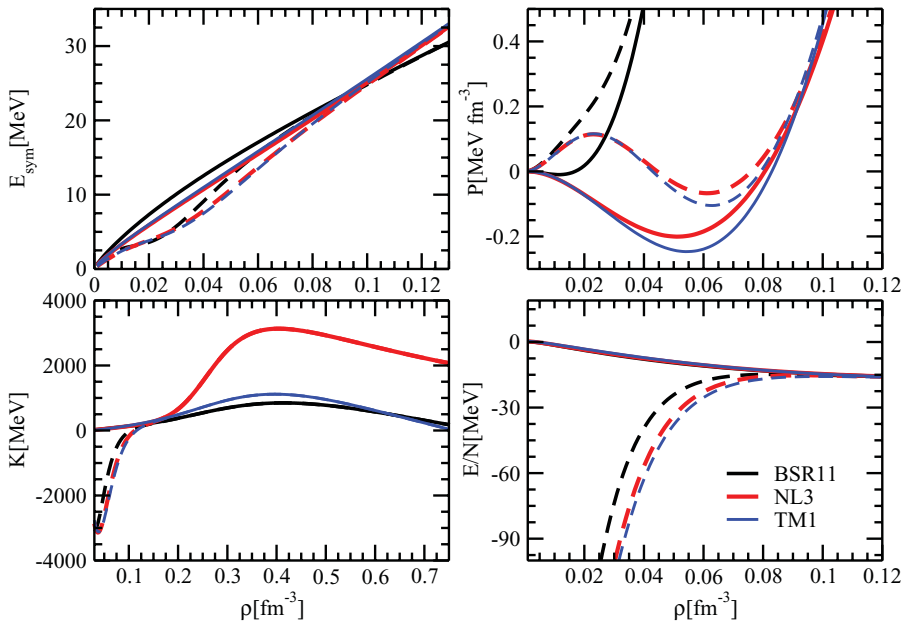

FIG. 8. (Color online) The comparison of the theoretical results for symmetry energy ($E_{\rm sym}$), the incompressibility coefficient (K), pressure (P), and energy per nucleon (E/A) computed with the BSR11 NL3 [27], and TM1 [28] parametrizations of relativistic mean-field theory at temperatures of 0 and 30 MeV as a function of density. The black lines represent the results of the BSR11 parametrization, the red lines represent the NL3 parametrization, and the blue lines represent the TM1 parametrization. The solid lines and the dashed lines represent temperatures of 0 and 30 MeV, respectively.

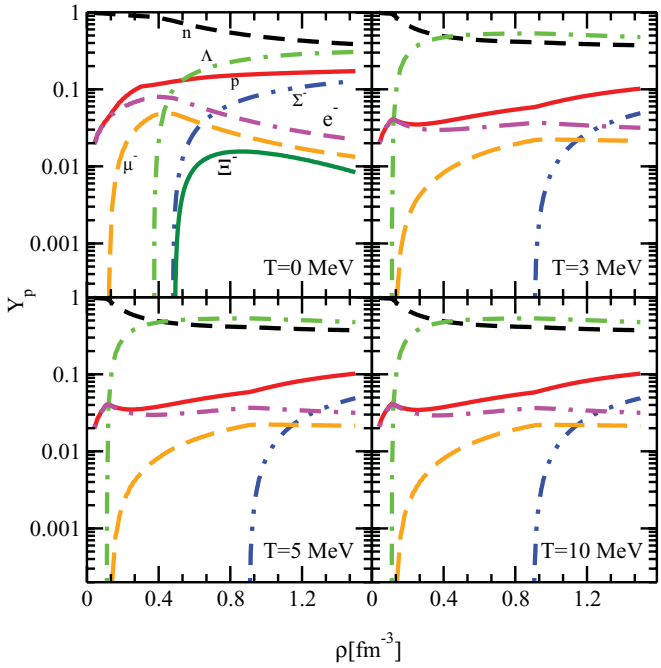

FIG. 9. (Color online) Relative particle fraction as a function of baryon density of the compact stars obtained for the BSR15 parametrization with the hyperon-meson coupling parameter $X_{\omega y} = 0.50$ at different temperatures.

constraint of the PSR J1614-2230 pulsar mass measurement and the prediction of its radius 11–15 km, where ζ is the

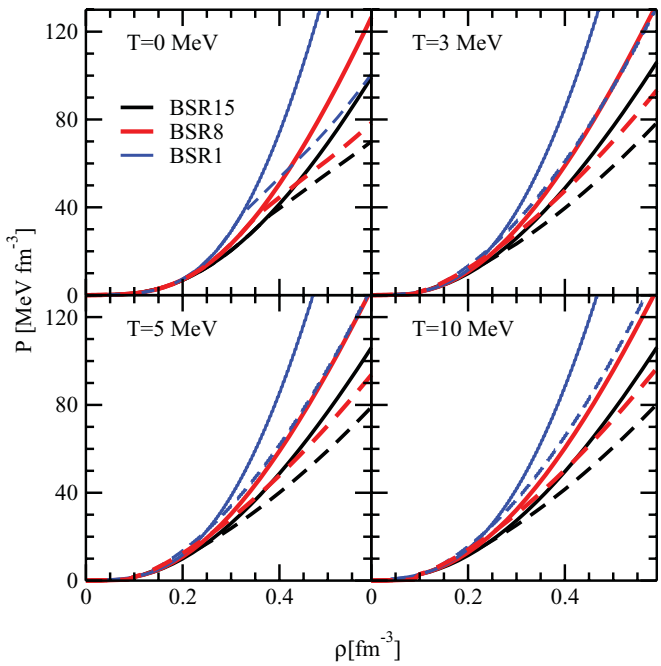

FIG. 10. (Color online) The pressure density is plotted as a function of density employing using the BSR1, BSR8, and BSR15 parametrizations. The dashed lines represent EOS with hyperons having the hyperon-meson coupling parameter $X_{\omega y} = 0.50$ and solid lines represent EOS without hyperons at temperatures of 0, 3, 5, and 10 MeV.

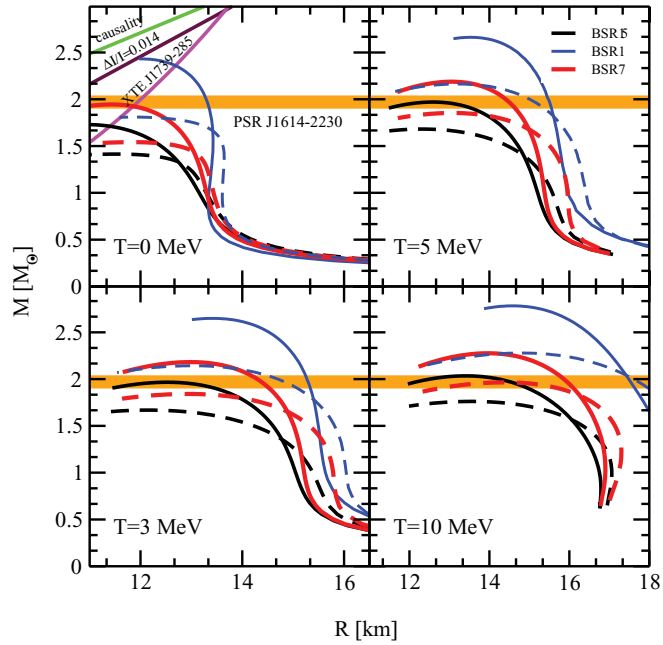

FIG. 11. (Color online) The mass and radius relationship of protoneutron stars. The dashed lines represent mass for EOS with hyperons having the hyperon-meson coupling parameter $X_{\omega y} = 0.50$, and the solid lines represent mass for EOS without hyperons at temperatures of 0, 3, 5, and 10 MeV. The colors blue, red, and black represent the BSR1, BSR8, and BSR15 parametrizations, respectively. The recent mass measurement of the PSR J1614-2230 pulsar is also displayed.

ω-meson self-coupling parameter, and mainly affects the high-density behavior of the EOS and cannot be constrained by the structural properties of finite nuclei measurements and bulk properties of nuclear matter at saturation density. From the argument of Tolman VII's solution of Einstein's equations for the relationship between maximum mass and its upper limit on the central energy density, we get the values [32] of $\epsilon_c = 1.92 \times 10^{15}$ g cm^{-3} and 2.73×10^{15} g cm^{-3} for the BSR1 and BSR15 parametrizations respectively. The EOS of warm dense nuclear matter becomes stiffer than the EOS of cold dense nuclear matter of the compact stars, even in the presence of exotic matter.

In Fig. 12 the maximum gravitational mass of PNS is plotted as a function of neutron skin thickness Δr in the ^{208}Pb nucleus at temperatures of 0, 3, 5, and 10 MeV. The color blue represents the mass computed with EOS without hyperons whereas red represents gravitational masses of EOS including hyperons, at $X_{\omega y} = 0.50$. Green and black represent masses of EOSs with hyperon; the values of $X_{\omega y}$ are equal to 0.60 and 0.70, respectively. The circles, triangles, and squares represent the values of maximum gravitational mass for the ω-meson self-coupling $\zeta = 0.0$, 0.03, and 0.06, respectively. We varied the hyperon-meson coupling parameter $X_{\omega y}$ from 0.50 to 0.70 at all temperatures and found that on increasing the coupling parameter the maximum gravitational mass of the PNS increased. It is noticed that the increase in gravitational mass of the compact star is large at $\zeta = 0.00$ and reasonably small at $\zeta = 0.06$. Further, Fig. 12 shows that the cold compact

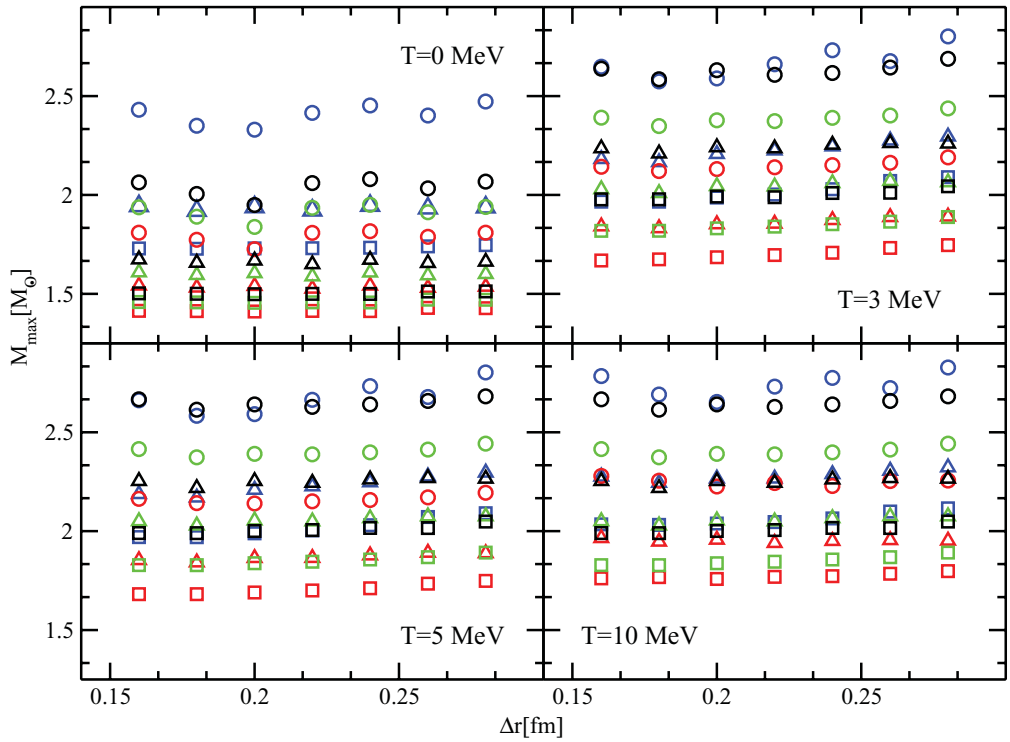

FIG. 12. (Color online) The maximum gravitational mass of a protoneutron star is plotted as function of neutron skin thickness (Δr) in the ^{208}Pb nucleus at temperatures of 0, 3, 5, and 10 MeV. The color blue represents the masses of EOS without hyperons, whereas the color red represents masses of EOS having hyperons with the hyperon-meson coupling parameter $X_{\omega y} = 0.50$. The colors green and black represent masses of EOS having hyperons with $X_{\omega y}$ 0.60 and 0.70, respectively. The circles, triangles, and squares represent the values of maximum gravitational mass for the ω-meson self-coupling $\zeta = 0.0$, 0.03, and 0.06, respectively.

star with hyperons can have gravitational mass $M \geqslant 2M_\odot$ if $\zeta = 0.00$ and $X_{\omega y} \geqslant 0.70$, whereas the PNS with hyperons can have mass $M \geqslant 2M_\odot$ if the chosen parameters are $\zeta = 0.00$ or 0.03 and $X_{\omega y} \geqslant 0.50$, and the compact star satisfies the constraint of the mass measurement of the PSR J1614-2230 pulsar [31].

In Tables II–IV we have presented the key structural properties of compact stars at finite temperatures; properties such as maximum gravitational mass, radius at maximum gravitational mass, radius for star with canonical mass ($1.4M_\odot$), and gravitational redshift of the photon $Z_{\rm surf}$ emitted from the compact star surface for a star with maximum mass and canonical mass using BSR1–BSR21 parametrizations at temperatures of 0, 3, 5, and 10 MeV without and with the inclusion of hyperons for $X_{\omega y} = 0.50$ only. It is observed from Tables II, III, and IV that with an increase in the value of the ζ parameter the mass of the compact star decreases, whereas with a rise in temperature the mass of the compact star increases. Further with increasing Δr the mass increases for all temperatures. It is also observed that when the temperature changes from 0 to 3 MeV there is an increase in the mass of the compact star by $\sim$0.2 to $0.4M_\odot$, but on further increasing the temperature to $T \geqslant 5$ MeV the increase in the mass of the compact star becomes very small. Also the increase in the radius at maximum mass and canonical mass ($M_{\rm max}$ and $M_{1.4}$) with temperature is $\sim$1.5–2 km initially but becomes smaller with further increases in temperature. The radius also increased with increasing Δr for all temperatures but decreased with increases in the value of the ζ parameter. The results for the gravitational redshift of the photon $Z_{\rm surf}$ emitted from the surface of the compact star can be computed as

$$Z_{\rm surf} = \left(1 - \frac{2GM}{Rc^2}\right)^{-1/2} - 1, \tag{17}$$

where R is the radius and M is the gravitational mass of the compact star. It is clear from Tables II, III, and IV that, with an increase in the ζ or Δr parameter, the gravitational redshift $Z_{\rm surf}$ and $Z_{1.4}$ decrease, whereas with an increase in temperature $Z_{\rm surf}$ and $Z_{1.4}$ decrease further. It is observed that the inclusion of hyperons in PNS decreases the magnitude of the mass, the radius, and the gravitational redshift for all RMF parametrizations. In comparison with cold compact stars, we obtained that the gravitational mass of the PNS with and without hyperons increases by $\sim 0.4M_\odot$, its radius increases by $\sim$3 km, and the radius $R_{1.4}$ at the canonical mass of the computed data increases by 3–6 km, whereas the value of the gravitational redshift at finite temperature decreases approximately 0.03–0.07.

C. Rotating PNS

The keplerian configurations of rapidly rotating PNS have been computed in the framework of general relativity by solving the Einstein field equations for stationary axisymmetric

TABLE II. The values of maximum gravitational mass M_{max}, radius R_{max}, radius $R_{1.4}$ corresponding to canonical mass $1.4M_{\odot}$, and the gravitational redshift of the photon emitted from the surface of the compact star at maximum mass Z_{max} and at canonical mass $Z_{1.4}$ for different values of the neutron skin thickness Δr at different temperatures for the ω-meson self-coupling $\zeta = 0.0$ with and without hyperons. The hyperon-meson coupling is $X_{\omega y} = 0.50$.

			Without hyperons					With hyperons				
Force	Δr	T	M_{max}	R_{max}	$R_{1.4}$	Z_{max}	$Z_{1.4}$	M_{max}	R_{max}	$R_{1.4}$	Z_{max}	$Z_{1.4}$
	(fm)	(MeV)	($M_{\odot}$)	(km)	(km)			($M_{\odot}$)	(km)	(km)		
BSR1	0.16	0	2.43	11.74	12.37	0.61	0.23	1.81	11.87	13.64	0.35	0.20
		3	2.65	13.11	14.12	0.58	0.19	2.14	12.53	14.49	0.42	0.18
		5	2.66	13.21	14.49	0.57	0.18	2.16	12.82	14.89	0.42	0.18
		10	2.78	14.61	18.82	0.51	0.13	2.28	14.81	19.30	0.35	0.13
BSR3	0.20	0	2.33	11.79	13.48	0.55	0.20	1.73	11.65	13.60	0.33	0.20
		3	2.59	13.43	15.62	0.52	0.17	2.13	13.16	16.03	0.38	0.16
		5	2.59	13.46	15.72	0.52	0.16	2.14	13.25	16.16	0.38	0.16
		10	2.65	14.11	17.06	0.50	0.15	2.23	14.30	17.56	0.36	0.14
BSR5	0.24	0	2.45	12.11	13.75	0.58	0.20	1.82	11.80	13.88	0.35	0.19
		3	2.73	13.83	16.00	0.55	0.16	2.15	13.26	16.19	0.39	0.16
		5	2.73	13.84	16.08	0.55	0.16	2.16	13.33	16.29	0.38	0.16
		10	2.78	14.30	17.22	0.53	0.15	2.23	14.30	17.56	0.36	0.14
BSR7	0.28	0	2.47	12.23	14.00	0.58	0.19	1.81	11.91	14.13	0.35	0.19
		3	2.80	14.29	16.57	0.54	0.15	2.19	13.71	16.69	0.38	0.15
		5	2.80	14.30	16.62	0.54	0.15	2.19	13.78	16.77	0.37	0.15
		10	2.83	14.60	17.47	0.53	0.14	2.26	14.59	17.77	0.37	0.14

space-time (e.g., see Ref. [33] and references therein). The numerical calculations have been performed by employing the rotating neutron star (RNS) code [34]. In Fig. 13 the mass shedding limit (Kepler) is plotted for EOS obtained by using the BSR1, BSR8, and BSR15 parametrizations at 0, 5, and 10 MeV in terms of gravitational mass M as a function of central energy density ϵ_c. The upper panel contains EOS without hyperons, whereas the lower panel contain EOS with hyperons at $X_{\omega y} = 0.50$. Keplerian configurations terminate at the central energy density where equilibrium solutions are stable with respect to the small axisymmetric perturbations; the slanting dotted (blue) line corresponds to the axisymmetric instability limit. In the Kepler limit sequences, the gravitational maximum mass of the PNS increase with increases in temperature by 20%–23% and its corresponding equitorial radius increases by 25%–46%, with respect to its nonrotating gravitational maximum mass and radius, respectively. These observations are reasonably well within the predictions provided in Refs. [33,35] and are slightly higher in the case of the PNS with hyperons. Compared with

TABLE III. Same as Table II but with ω-meson self-coupling $\zeta = 0.03$.

			Without hyperons					With hyperons				
Force	Δr	T	M_{max}	R_{max}	$R_{1.4}$	Z_{max}	$Z_{1.4}$	M_{max}	R_{max}	$R_{1.4}$	Z_{max}	$Z_{1.4}$
	(fm)	(MeV)	($M_{\odot}$)	(km)	(km)			($M_{\odot}$)	(km)	(km)		
BSR8	0.16	0	1.94	11.43	13.08	0.42	0.21	1.54	11.82	13.14	0.28	0.21
		3	2.18	12.99	15.07	0.41	0.17	1.84	12.92	15.50	0.31	0.17
		5	2.19	13.05	15.21	0.41	0.17	1.85	13.07	15.68	0.31	0.17
		10	2.28	13.96	16.78	0.39	0.15	1.96	14.39	17.24	0.30	0.15
BSR10	0.20	0	1.94	11.46	13.19	0.41	0.21	1.54	11.80	13.24	0.28	0.21
		3	2.21	13.20	15.43	0.41	0.17	1.85	13.04	15.72	0.31	0.17
		5	2.21	13.24	15.53	0.41	0.17	1.86	13.16	15.86	0.31	0.16
		10	2.27	13.91	16.86	0.39	0.15	1.96	14.31	17.32	0.30	0.15
BSR12	0.24	0	1.95	11.49	13.29	0.42	0.21	1.54	11.84	13.33	0.27	0.20
		3	2.25	13.43	15.73	0.41	0.16	1.87	13.23	15.92	0.31	0.16
		5	2.25	13.45	15.80	0.41	0.16	1.88	13.31	16.03	0.31	0.16
		10	2.29	14.00	16.94	0.39	0.15	1.95	14.30	17.35	0.29	0.15
BSR14	0.28	0	1.94	11.54	13.51	0.41	0.20	1.54	11.89	13.53	0.27	0.20
		3	2.30	13.82	16.20	0.40	0.16	1.89	13.45	16.21	0.31	0.16
		5	2.30	13.84	16.25	0.40	0.16	1.89	13.48	16.29	0.31	0.16
		10	2.32	14.25	17.15	0.39	0.15	1.95	14.36	17.44	0.29	0.15

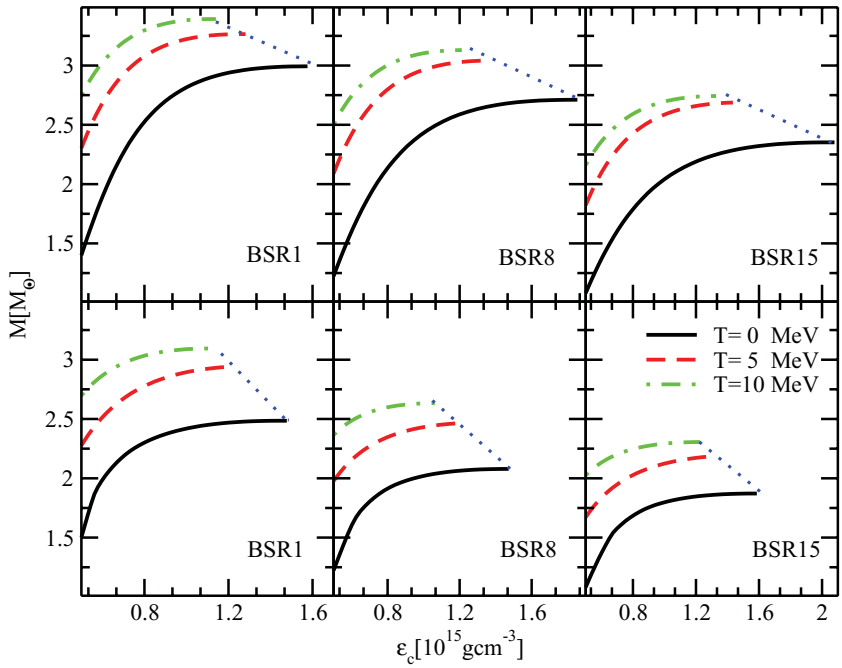

FIG. 13. (Color online) The mass shedding limit (Kepler) is plotted for EOS obtained using BSR1, BSR8, and BSR15 parametrizations at temperatures of 0, 5, and 10 MeV in terms of gravitational mass M as a function of central energy density ϵ_c. The upper panels contain EOS without hyperons, whereas the lower panels contain EOS with hyperons having the hyperon-meson coupling parameter $X_{\omega y} = 0.50$. The slanting dotted (blue) line corresponds to the axisymmetric instability limit.

the cold nuclear matter compact star, the Keplerian angular velocity of the PNS decreases by 5%–8% in the case of the PNS without hyperons, and it is 14%–20% for the PNS with hyperons.

IV. CONCLUSION

The effect of temperature and density dependence of the asymmetric nuclear matter properties is studied within the ERMF model which includes the contribution from the self and mixed interaction terms by using different parametrizations obtained by varying the neutron skin thickness Δr and the ω-meson self-coupling (ζ). We studied the bulk properties of cold and warm nuclear dense matter at finite temperature and compared the structural properties of nonrotating and rotating cold compact stars with PNS constructed within the ERMF model.

We observed that the changes in bulk properties at saturation densities are negligible till a temperature of 20 MeV but as temperatures increase further these properties start varying significantly. It is found that variation in the values of symmetry energy becomes reasonably large as the value of the neutron skin thickness increases, whereas the value for the slope of symmetry energy remains unaffected at $T = 0$ and 30 MeV. The value of the incompressibility coefficient is

TABLE IV. Same as Table II but with ω-meson self-coupling $\zeta = 0.06$.

			Without hyperons					With hyperons				
Force	Δr	T	$M_{\max}$	$R_{\max}$	$R_{1.4}$	$Z_{\max}$	$Z_{1.4}$	$M_{\max}$	$R_{\max}$	$R_{1.4}$	$Z_{\max}$	$Z_{1.4}$
	(fm)	(MeV)	($M_\odot$)	(km)	(km)			($M_\odot$)	(km)	(km)		
BSR15	0.16	0	1.73	10.92	12.62	0.37	0.22	1.41	11.52	12.15	0.25	0.23
		3	1.97	12.53	14.73	0.37	0.18	1.67	12.14	14.64	0.30	0.18
		5	1.97	12.60	14.86	0.36	0.18	1.68	12.31	14.85	0.30	0.18
		10	2.03	13.41	16.36	0.35	0.16	1.76	13.54	16.64	0.27	0.15
BSR17	0.20	0	1.73	10.93	12.66	0.37	0.22	1.41	11.49	12.09	0.25	0.23
		3	1.99	12.66	14.95	0.37	0.18	1.69	12.33	14.88	0.30	0.18
		5	1.99	12.70	15.04	0.36	0.17	1.69	12.44	15.03	0.29	0.17
		10	2.04	13.38	16.40	0.35	0.16	1.76	13.56	16.71	0.27	0.15
BSR19	0.24	0	1.73	11.01	12.83	0.37	0.22	1.41	11.56	12.24	0.25	0.23
		3	2.03	12.99	15.41	0.36	0.17	1.71	12.61	15.26	0.29	0.17
		5	2.03	13.04	15.48	0.36	0.17	1.71	12.69	15.38	0.29	0.17
		10	2.06	13.56	16.62	0.35	0.15	1.77	13.73	16.90	0.27	0.15
BSR21	0.28	0	1.75	11.17	13.13	0.36	0.21	1.43	11.69	12.68	0.25	0.22
		3	2.09	13.49	15.97	0.36	0.16	1.75	12.96	15.77	0.29	0.16
		5	2.09	13.51	16.02	0.36	0.16	1.75	13.02	15.84	0.29	0.16
		10	2.12	13.91	16.92	0.35	0.15	1.80	13.88	17.11	0.27	0.15

sensitive to ζ and indicates the change at $T = 30$ MeV. The energy per nucleon for symmetric nuclear matter decreases sharply as compared to the energy for pure neutron matter at very low densities, and upon increasing the ζ the decrease becomes moderate whereas upon increasing Δr the value remains almost the same. It is observed that with the increase in the asymmetry parameter δ, the EOS become stiff and the trend continues until it becomes pure neutron matter. It is found that the temperature dependence of the symmetry energy is more sensitive to the small values of Δr. Although the symmetry energy decreases with increases in temperature, at very low density ($\sim$0.02 fm^{-3}) the trend reverses.

In our calculations at finite temperature, neutrons, protons, Λ hyperons, and electrons become abundant at baryon density lower than their particle threshold density in the cold nuclear matter, whereas Ξ hyperons disappear even at $T = 3$ MeV. The EOS of warm dense nuclear matter becomes stiffer than the EOS of the cold dense nuclear matter of the compact stars, even if we include the exotic matter. We varied the hyperon-meson coupling parameter $X_{\omega y}$ from 0.50 to 0.70 at all temperatures and found that on increasing the coupling parameter the maximum gravitational mass of the star increased and this increase was large for the smaller values of ζ and small for the larger values of ζ. Values of all the properties such as mass, radius, and gravitational redshift decreased upon inclusion of hyperons for all the parametrizations. We obtained that the gravitational mass of the PNS with and without hyperons increased by $\sim 0.4 M_{\odot}$ and its radius increased by $\sim$3 km, and the radius $R_{1.4}$ at the canonical mass of the computed data increased by 3–6 km, whereas the value of the gravitational redshift at finite temperature decreased approximately 0.03–0.07. In the Kepler limit sequences, the gravitational maximum mass of PNS increased with increases in temperature by 20%–23% and its corresponding equitorial radius increased by 25%–46%, with respect to its nonrotating gravitational maximum mass and radius, respectively. The Keplerian angular velocity of PNS without hyperons decreased by 5%–8% and it decreased by 14%–20% for PNS with hyperons, in comparison to the cold CS without and with hyperons, respectively.

[1] E. Chabanat, P. Bonche, P. Haensel, J. Meyer, and R. Schaeffer, Nucl. Phys. A **627**, 710 (1997).
[2] J. R. Stone, J. C. Miller, R. Koncewicz, P. D. Stevenson, and M. R. Strayer, Phys. Rev. C **68**, 034324 (2003).
[3] B. K. Agrawal, S. K. Dhiman, and R. Kumar, Phys. Rev. C **73**, 034319 (2006).
[4] A. W. Steiner, M. Prakash, J. M. Lattimer, and P. Ellis, Phys. Rep. **411**, 325 (2005).
[5] J. D. Walecka, Ann. Phys. (NY) **83**, 491 (1974).
[6] P. Ring, Prog. Part. Nucl. Phys. **37**, 193 (1996).
[7] J. Meng and P. Ring, Phys. Rev. Lett. **77**, 3963 (1996).
[8] L. W. Chen, C. M. Ko, and B. A. Li, Phys. Rev. C **72**, 064309 (2005).
[9] L. W. Chen, C. M. Ko, and B. A. Li, Phys. Rev. C **76**, 054316 (2007).
[10] B. A. Li, L. W. Chen, and C. M. Ko, Phys. Rep. **464**, 113 (2008).
[11] T. Li *et al.*, Phys. Rev. Lett. **99**, 162503 (2007).
[12] D. H. Youngblood, H. L. Clark, and Y. W. Lui, Phys. Rev. Lett. **82**, 691 (1999).
[13] Z. Y. Ma, A. Wandelt, N. V. Giai, D. P. Ring, and L. G. Cao, Nucl. Phys. A **703**, 222 (2002).
[14] D. V. Shetty, S. J. Yennello, and G. A. Souliotis, Phys. Rev. C **75**, 034602 (2007).
[15] J. B. Natowitz *et al.*, Phys. Rev. Lett. **104**, 202501 (2010).
[16] M. B. Tsang, Y. Zhang, P. Danielewicz, M. Famiano, Z. Li, W. G. Lynch, and A. W. Steiner, Phys. Rev. Lett. **102**, 122701 (2009).
[17] S. Yoshida, H. Sagawa, and N. Takigawa, Phys. Rev. C **58**, 2796 (1998).
[18] T. Li *et al.*, Phys. Rev. C **81**, 034309 (2010).
[19] H. Shen, Phys. Rev. C **65**, 035802 (2002).
[20] H. J. Schulze, A. Polls, A. Ramos, and I. Vidana, Phys. Rev. C **73**, 058801 (2006).
[21] S. L. Shapiro and S. A. Teukolsky, *Black Holes, White Dwarfs and Neutron Stars* (Wiley, New York, 1983).
[22] N. K. Glendenning, *Compect Stars: Nuclear Physics, Particle Physics, and General Relativity* (Springer-Verlag, New York, 2000).
[23] S. Balberg, I. Lichtenstadt, and G. B. Cook, Astrophys. J. Suppl. **121**, 515 (1999).
[24] S. K. Dhiman, R. Kumar, and B. K. Agrawal, Phys. Rev. C **76**, 045801 (2007).
[25] B. D. Serot and J. D. Walecka, Int. J. Mod. Phys. E **6**, 515 (1997).
[26] B. K. Agrawal, Phys. Rev. C **81**, 034323 (2010).
[27] G. A. Lalazissis, J. Konig, and P. Ring, Phys. Rev. C **55**, 540 (1997).
[28] Y. Sugahara and H. Toki, Nucl. Phys. A **579**, 557 (1994).
[29] G. Baym, C. Pethick, and P. Sutherland, Astrophys. J. **170**, 299 (1971).
[30] S. Weinberg, *Gravitation and Cosmology* (Wiley, New York, 1972).
[31] P. B. Demorest, T. Pennucci, S. M. Ransom, M. S. E. Roberts, and J. W. T. Hessels, Nature (London) **467**, 1081 (2010).
[32] S. K. Dhiman, G. Mahajan, and B. K. Agrawal, Nucl. Phys. A **836**, 183 (2010).
[33] N. Stergioulas, Living Rev. Rel. **6**, 3 (2003).
[34] N. Stergioulas and J. L. Friedman, Astrophys. J. **444**, 306 (1995).
[35] J. O. Goussard, P. Haensel, and J. L. Zdunik, Astron. Astrophys. **321**, 822 (1997).